Applied Materials Today 20 (2020) 100740

Contents lists available at ScienceDirect

Applied Materials Today

journal homepage: www.elsevier.com/locate/apmt

Strain-polarization coupling mechanism of enhanced conductivity at the grain boundaries in $BiFeO_3$ thin films

Denis Alikin[a], Yevhen Fomichov[b], Saulo Portes Reis[c,d], Alexander Abramov[a], Dmitry Chezganov[a], Vladimir Shur[a], Eugene Eliseev[e], Sergei V. Kalinin[f], Anna Morozovska[g], Eudes B. Araujo[c], Andrei Kholkin[h,*]

[a] School of Natural Sciences and Mathematics, Ural Federal University, 620100, Ekaterinburg, Russian Federation
[b] Faculty of Mathematics and Physics, Charles University in Prague, Prague 8, 180 00, Czech Republic
[c] Department of Chemistry and Physics, São Paulo State University, Ilha Solteira, SP, Brazil
[d] Federal Institute of Education, Science and Technology of São Paulo, 15503-110 Votuporanga, Brazil
[e] Institute for Problems of Materials Science, National Academy of Sciences of Ukraine, 03142 Kyiv, Ukraine
[f] Institute of Physics, National Academy of Sciences of Ukraine, 03028 Kyiv, Ukraine
[g] Center for Nanophase Materials Sciences, Oak Ridge National Laboratory, Oak Ridge, TN 37831, USA
[h] Department of Physics & CICECO-Aveiro Institute of Materials, 3810-193, University of Aveiro, Portugal

ARTICLE INFO

Article history:
Received 17 February 2020
Revised 27 May 2020
Accepted 21 June 2020

Keywords:
bismuth ferrite
grain boundaries
conductivity
interfaces
domain structure

ABSTRACT

Charge transport across the interfaces in complex oxides attracts a lot of attention because it allows creating novel functionalities useful for device applications. It has been observed that movable domain walls in epitaxial $BiFeO_3$ films possess enhanced conductivity that can be used for reading out in ferroelectric-based memories. In this work, the relation between the polarization, strain and conductivity in sol-gel $BiFeO_3$ films with special emphasis on grain boundaries as natural interfaces in polycrystalline ferroelectrics is investigated. The interaction between polarization and grain boundaries occuring at elevated temperatures during or after material sintering stage leads to the formation of branched network of highly conductive grain boundaries with the electrical conductivity about two orders higher than in the bulk. At room temperature, these conductive traces stabilized by the defects remain and do not change upon polarization switching. These collective states provide further insight into the physics of complex oxide ferroelectrics and may strongly affect their practical applications, because reveal an additional mechanism of the leakage current in such systems.

1. Introduction

Complex oxides are attracting considerable attention because of their ferroelectric, ferromagnetic, multiferroic, and other remarkable properties, which are of great interest for the modern microelectronic and micromechanical devices. The macroscopic properties of these materials depend strongly on the composition, defect state and transport across various interfaces [1–5]. Many efforts have been devoted so far to control the physical properties of the interfaces in ferroelectric materials by their polarization state. These efforts resulted in the discovery of a variety of different phenomena such as polarization-dependent tunneling effect, resistive switching, symmetry breaking, etc. [6,7]. In particular, domain wall conductivity, [8–10] formation of topological defects [11,12], phase boundaries [13], and ferroelectric-insulator interfaces [14] have been rigorously studied. In general, the control of local conductivity along these interfaces can be engineered based on the mutual orientation of adjacent polarization states [12,14]. The effect of enhanced conductivity at polar interfaces of different nature has been discovered at the interface between two insulating oxides [15,16] and charged domain walls in ferroelectrics [17,18]. The value of the enhanced current and properties of 2D electron gas were polarization-dependent and polarization reversal could be used to create and erase the conductive states [17]. However, to the best of our knowledge, no studies of the polarization-dependent conductivity in more complex polycrystalline ferroelectric materials have been undertaken so far. Currently, thin film materials and nanostructures offer significant advantages for device fabrications, as exemplified by high recording density magnetic media, memristors, ferroelectric memories, etc. While several studies have been devoted to ferroelectric phenomena at single grain boundaries

* Corresponding author.
E-mail address: kholkin@ua.pt (A. Kholkin).

https://doi.org/10.1016/j.apmt.2020.100740
2352-9407/

[19–25] and a few studies to the collective phenomena in polycrystalline thin films [26–32], the interaction of domain wall and grain boundary subsystem and collective phenomena emerging in such system has not yet been explored.

Polycrystalline ferroelectric materials are known to possess macroscopic properties significantly entangled by their structural heterogeneity caused not only by the existence of domains and domain walls, but also by the complicated grain and phase boundary interfaces, large macroscopic defects, e.g. dislocations, etc. The domain wall contribution to the functional properties such as dielectric constant and piezoelectric coefficient was only approximately estimated and it was thought to be about 50–70% of the total response [33,34]. At the same time, domain walls in polycrystalline ferroelectrics are expected to behave differently as compared to single crystals. Domains appear to be mechanically clamped inside individual grains, [35,36] and grain boundaries effectively pin the domain walls and limit their motion. [37–40] From the very beginning, domain structure in the coarse-grain bulk ceramics is known to be organized in peculiar domain patterns, representing individual domain "bands" containing ferroelastic and ferroelectric domain walls. [35] Similar phenomena of the domain wall organization into the individual clusters, so-called "superdomains", have been observed in thin films [29]. The applied electric field causes collective behavior of such domain structure and its correlated response determines many functional properties. [28,29]

In single crystals or epitaxial thin films, polarization-dependent domain wall conductivity is closely connected to the polarization screening [8,41]. Domain walls joining adjacent domain states are conductive mainly due to polarization charge localized in them [41,42]. The conductivity across domain walls rapidly relaxes after polarization reversal due to the screening by the external charge carriers [18,43] Domain walls conductivity is also dependent on the domain wall tilt changing continuously during forward domain propagation [9,44–46]. Additional enhancement of conductivity can occur due to interaction between domain walls and structural defects often resulting in more complex domain systems existing in polycrystalline films and bulk ceramics [9,47]. Intriguing possibility to control domain wall properties via defect engineering, e.g., by the annealing in a controllable atmosphere has been recently demonstrated in $BiFeO_3$ (BFO) ceramics [47].

In polycrystalline ferroelectrics, grain boundaries (GBs) are formed at the stage of materials synthesis at elevated temperature, when the accelerated diffusion of mobile species occurs during grain growth and their mechanical consolidation. At room temperature, GBs become stable and represent mostly 2D defects with different from the bulk electronic and ionic transport properties caused by the structural and chemical disorder [48–50]. Thereby, they impact directly on the leakage currents, breakdown strength, dielectric permittivity, and piezocoefficients of the ferroelectric polycrystalline materials (e.g., may act as conductive inclusions effectively influencing dielectric losses or potential barriers for the electronic or ionic transport) [51–53]. The segregation of various defects and/or impurities in the vicinity of GBs provides also a discontinuity of chemical potential and counterbalances intergranular strain [47,54,55].

In this work, we study the appearance of collective polarization and transport phenomena as a result of an interaction between GBs and domain walls in polycrystalline sol-gel synthesized BFO films. We found that these grains self-organize in mesoscale clusters (superdomains) with uniform polarization comprising a number of grains, resulting in non-trivial collective effects resembling formation of the clusters of non-linear electro-mechanical response in polycrystalline films [28]. These boundaries become conductive and thus control the transport phenomena in BFO films. Since conventional mechanism of stress compensation by the formation of ferroelastic domain walls is not likely for fine grains, we argue that the accumulation of stress at elevated temperature triggers local polarization to be organized in clusters. We show that the enhanced electric and elastic fields at the GBs lead to local bending of the conduction and valence bands sourced by flexoelectric effect and result in the increased conductivity of the grain boundaries. This process apparently happens at elevated temperatures, at which defects are sufficiently mobile and can interact with conductivie interfaces, while at room temperature the conductive traces become frozen, and conductivity controlled by the immobile charged defects conserves.

2. Materials and methods

$BiFeO_3$ thin films were deposited on $Pt/TiO_2/SiO_2/Si(100)$ substrates by spin coating using a chemical solution with 7.5 mol% of excess bismuth. The 0.16 M solution was obtained by the dissolution of $Bi(NO_3)_3 \bullet 5H_2O$ and $Fe(NO_3)_3 \bullet 9H_2O$ in 2-methoxyethanol and glacial acetic acid at 50 °C for 10 min. The films were then crystallized in air at 600 °C for 40 min to obtain a final film of ~ 500 nm thickness. The heating and cooling were done with a 5 °C /min rate.

The crystal structure of the $BiFeO_3$ film was characterized by X-ray diffraction (XRD) using a Rigaku Ultima IV diffractometer with CuKα (λ = 1.5406 Å) radiation. A typical perovskite structure randomly oriented without secondary phases was observed in the XRD pattern. Considering the R3c space group for the BFO system, Rietveld refinements were conducted to analyze the diffractograms. The lattice parameters and other structural parameters agree with the results for similar BFO thin films in the literature. Raman measurements were performed using a confocal Raman BX51-Voyage^{TM} with laser power of 150 mW, excitation of 785 nm, and spectral resolution of 3 cm^{-1}. Within 13 active Raman-modes predicted by the group theory, 12 Raman modes were observed in polycrystalline BFO films studied in the present work. Both XRD and Raman results are summarized in Supplementary Information A.

Piezoresponse Force Microscopy (PFM) was done using a MFP-3D-SA (Asylum Research, Oxford Instruments, UK) scanning probe microscope with NT-MDT NSG 01 commercial tips with Pt coating, 35 nm nominal tip radius, about 5 N/m spring constant, and 150 kHz free resonance frequency. The visualization of domain structure by PFM was done at 20 kHz excitation frequency that is far from the frequency of the first contact resonance (higher than 450 kHz). Vertical and lateral PFM signals were quantified based on the measurements of the vertical and lateral force-distance curves, respectively, as described in Refs. [56–58].

Local conductivity measurements were done in the incorporated "Spreading Resistance" mode of NTEGRA Aura microscope in dark conditions and under 365 nm UV illumination by the photodiode light focused on the sample with about 100 mW/cm^2 power density. DC voltage (up to 10 V) was applied to NT-MDT VIT_P/Pt tips with "top-visual" geometry allowing to illuminate the samples, with 30 nm nominal tip radius, 50 N/m spring constant, and 300 kHz free resonance frequency. Atomic Force Microscopy (AFM) photodiode was screened from the UV light by the suitable optical filter. We used photo-illumination during current aqusition to get better signal-to-noise ratio of the images allowing to distinguish details of the current distribution. As we demonstrated in the Supplementary Information B the Conductive AFM (C-AFM) contrast at the GBs was identical for both dark and UV-illuminated conditions. C-AFM contrast of the GBs captured at the forward and backward pass of the scanner repeated each other. The value of the current was constant in time in any point of the scan. This unambiguously identifies that steady state conditions were achieved during scanning.

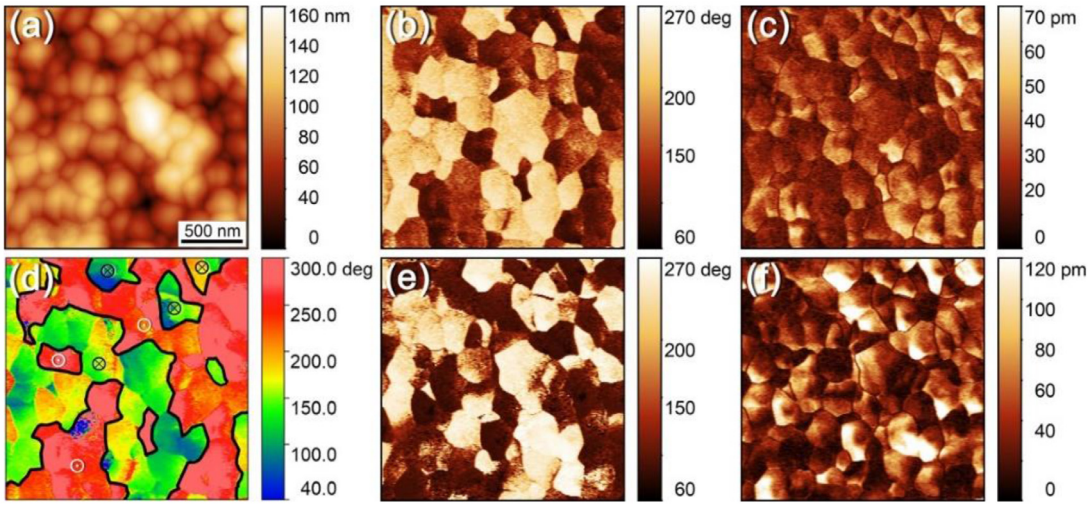

Fig. 1. Ferroelectric domain structure in BFO thin films: (a) topography, (b) vertical PFM phase, (c) vertical PFM amplitude, (d) vector PFM phase extracted according to the methodology described in Ref [60]. with cluster boundaries and out-of-plane polarization direction marked by the black lines and symbols, (e) lateral PFM phase, (f) lateral PFM amplitude.

Scanning Probe Microscopy measurements were realized in dry argon atmosphere via the constant flow of the argon gas. The measurements were done on the series of the samples grown under similar experimental conditions.

Electron backscattered diffraction (ESBD) measurements were carried out using 20 kV accelerating voltage and 5 nA electron beam current on Carl Zeiss Auriga Workstation equipped with Oxford Instruments Channel5 system. The sample was covered with about 2 nm carbon layer before the measurements to avoid surface charging and polarization reversal by the electron beam. The area of 200•200 μm^2 was scanned with a 20–50 nm step size. Electron back-scattering patterns were collected by the NordlysF+ EBSD detector and analyzed by the Flamenco acquisition software. The local texture analysis was done by the Mambo software.

3. Results and discussion

3.1. Clustering of the polarization and polarization-dependent conductivity

To explore the interplay between transport properties mediated by the domain walls and grain boundaries, we studied domain structure and local conductivity simultaneously by vector PFM and C-AFM, respectively We observed clear piezoresponse contrasts both in lateral and vertical PFM signals (Fig. 1) that were expected for the multiaxial ferroelectric material with rhombohedral crystal symmetry. We found that the individual grains were all single domain and did not contain any domain walls inside the grains, which indicates that the grain size was less than the critical size, at which the screening of depolarization field makes single-domain state energetically preferable [59]. Surprisingly, we found self-organized arrangement of the domain structure confined in "clusters" with the correlated orientation of spontaneous polarization. This follows from the distribution of the vertical and lateral PFM phase signals that is not random. Using the methodology described in Ref. [60] vector PFM map was constructed (see Fig. 1d), where clusters with the same sign of the piezoresponse (i.e. up or down polarization directions) are highlighted. Vector PFM approach combines both in-plane and out-of-plane PFM signals to reconstruct preferred orientation of polarization vector in the azimuthal plane [60]. From the comparison of Figs. 1b, 1d and 1e, it can be seen that vector PFM phase contrast is mostly out-of-plane, so the polarization prefers vertical (out of the film's plane)

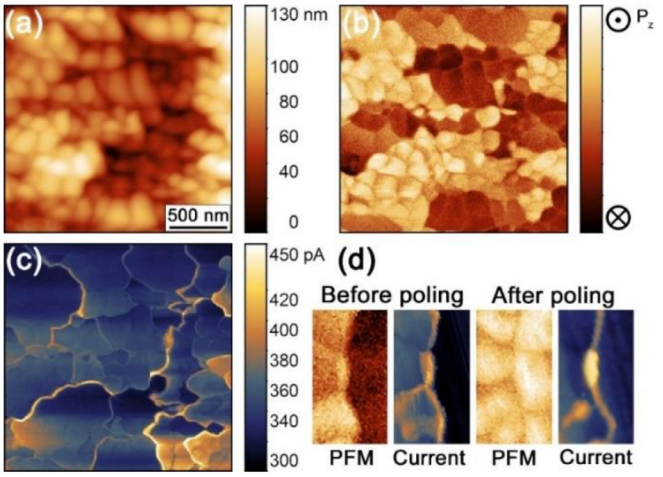

Fig. 2. Correlation between piezoresponse and conductivity in BFO thin films: (a) topography, (b) PFM response, (c) electric current, (d) conductive grain boundary before and after poling by the tip scanning with 20 V DC voltage applied.

orientation. Such preferably oriented clusters usually consist of 3–20 grains. The cluster size varies across the sample, which indicates that the driving force for their formation is non-uniformly distributed over the surface.

Rigorous analysis of electron backscattering diffraction patterns confirmed non-uniform distribution of Euler angles of the poled figures with preferable orientation in the out-of-plane direction (Supplementary Information C, Figures C1 and C2). It means a decrease of the ratio between the out-of-plane and in-plane domains, so that some "self-poling" occurs in the films [61]. It must be noted that EBSD images treated by the kinematic theory cannot reveal 180-degree domains [62] and, thereby, are not able to show domain clusters observed by PFM. Self-poling has been earlier revealed in BFO thick films (tens of microns thick), [63] as well as in PZT sol-gel films. [61] Formation of domain clusters in our case can be called local "self-poling" effect because preferred orientation of spontaneous polarization occurs only at the mesoscale.

We further explore the features of the electronic transport in BFO films with such organized domain structure by C-AFM (Fig. 2). Current varies significantly at the GBs in the interior of the do-

main clusters and at their circumference. The GBs at the cluster circumference were mostly highly conductive, while the electrical conductivity of GBs localized inside the clusters was similar to that in the bulk. The current measured by C-AFM on conductive GBs was 30–100 times higher than in the bulk, suggesting comparable increase of the conductivity.

In BFO epitaxial films, the domain walls are known to be more conductive than the bulk and this effect can be controlled by the electric field. [8–10] The conductivity increase was earlier rationalized by the local decrease of the bandgap under the action of free charge carriers trapped at the domain walls [8–10]. Later, strong angular dependence of the carrier accumulation was suggested to originate from the local band bending via angle-dependent electrostriction and flexoelectric coupling mechanisms [64].

In order to further underpin the mechanism of conductivity variation in our films we performed local switching experiments (Fig. 2d). The application of a DC bias higher 12 V by the AFM tip can easily switch the out-of-plane direction of polarization either in single grains or inside a large area by scanning under DC bias (Supplementary Information D, Fig. D1). However, uniform local poling of the area at the position of the conductive GB under 20 V does not significantly change the current distribution and enhanced conductivity was not obesrved at the boundary of the poled area (Supplementary Information D, Fig. D1). This indicates that the observed effect is different as compared to epitaxial BFO films [8,9] in which conductivity along domain walls is induced under poling. Thereby, the conductivity in polycrystalline BFO films should be linked to the properties of GBs.

According to generally accepted model [49] GBs consist of the defective 1–2 nm-thick “core” region, where most of the defects are segregated, while the neighboring region of 30–50 nm width becomes depleted by the charge carriers. Depending on the defect chemistry of the material, major or minor charge carriers can be segregated at the GBs [48,49], thereby enhancing of reducing their conductivity. Defect chemistry of pure BFO ceramics is still under discussion, mainly because of the large contribution of interface-controlled conductivity to macroscopic materials properties [47,65]. Epitaxial films were shown to be *n*-type electronic conductors with the domain walls of the same conductivity type [10,66]. Ceramics and polycrystalline BFO films were reported both *n*- and *p*-type [47,65,67,68]. Recent scanning electron transmission microscopy of the undoped polycrystalline BFO ceramics revealed segregation of Bi vacancies near domain walls [47]. The annealing in N_2 atmosphere was shown to suppress conductivity across the domain walls, which was suggested to be *p*-type and meditated by the electron-hole hopping between Fe^{4+} and Fe^{3+} sites. Schrade et al. [65] studied electron transport mechanisms in bulk BFO ceramics by measuring both electrical conductivity and Seebeck coefficient simultaneously at different temperatures and oxygen partial pressures. Contrary to Rojac et al. [47], they found undoped BFO to be close to intrinsic conductivity, $n = p$, with an additional contribution attributed to parallel electronic transport along the domain wall interfaces. The charge compensation mechanism was suggested to be the Bi vacancies compensated by the oxygen vacancies [65].

Based on the activation energy of electronic transport extracted from the temperature-dependent dielectric measurements the conductivity across the grain bulk and resistive (intra-cluster) GBs is attested to *n*-type small-polaron hopping, because the obtained activation energy 0.08–0.11 eV is lower than the typical activation energy for the holes (around 0.2 eV [65,67]) (see Supplementary Information E). The conductivity is likely deviates from the intrinsic behavior as a result of the formation of the oxygen or bismuth vacancies caused by the volatilization of Bi [69,70]. It is reasonable to conclude that the GBs with enhanced conductivity contain another type of the segregated defects responsible for the enhanced conductivity, e.g. negatively charged Bi vacancies providing *p*-type conductivity (as it was found for the $BiFeO_3$ ceramics [47]).

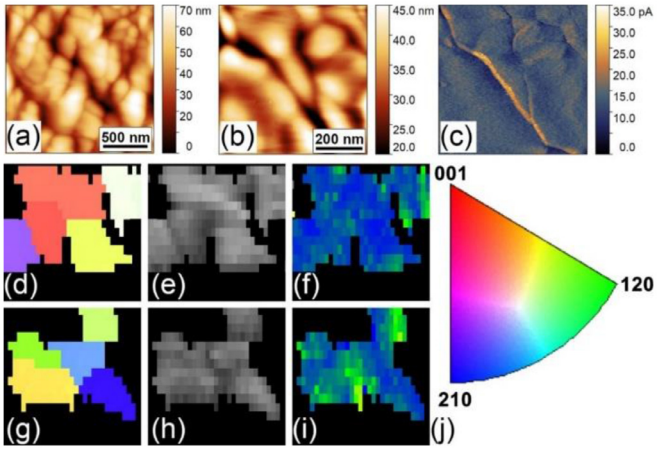

Fig. 3. (a) and (b) Topography, (c) CAFM and (d-i) EBSD images (5·5 μm^2 size) of the grain agglomerates in polycrystalline BFO sol-gel thin films. (d-f) and (g-i) Two different places across the surface. (d, g) Inverse polar figure (IPF) Z maps, (e, h) image quality (band contrast) maps, (f,i) local misorientation maps. (j) Color map for IPF Z contrasts in (d, g). Relative intensities of the image quality and local misorientation maps are chosen the same for reliable comparison.

The resolution of C-AFM is not enough to distinguish the conductivity of the core and depleted area of the conductive GB and reconstruct its detailed structure. Nevertheless, the effect of the formation of the double-charged defect layer across the interface with polarization charge was predicted by modeling [71,72], as well as conductive traces at the positions of the domain walls were observed experimentally in the epitaxial BFO films after polarization reversal [73]. Thus, the segregation of the defects at the polar interfaces happens as a result of the depolarization field screening at the interface in order to minimize the energy of the system [74]. It likely occurs at the high-temperature stage of the materials synthesis, because defects are highly mobile at elevated temperature and can effectively take part in the screening process. At room temperature, the segregated defects become immobile and cannot rapidly follow the polarization change. Consequently, polarization reversal at room temperature does not lead to the immediate elimination of the conductivity along the GBs.

One of the possible reasons of the enhanced conductivity at the interface is a coupling between polarization and stress occuring at the GBs, which results in the mechanical strain. Indeed, domain clusters in BFO films often demonstrate a visible separation in topography with pronounced cracks between different crystallites (Fig. 3a). Exactly these positions in the studied sample possess enhanced conductivity (Fig. 3). We used EBSD to study the grain agglomerates with preferable orientation in out-of-plane direction GBs across the sample (Fig. 3d-i). In Fig. 3d-i two typical agglomerates are shown (top and bottom image panels). Local orientation contrast (Fig. 3f,i) and image quality (Fig. 3e,h) in the middle of the agglomerate (exactly at the GB position) is stronger for the bottom panel. These parameters (image quality and local misorientation) reflect an apparent concentration of the mechanical strain [75,76]. This behavior cannot be attributed to any artifact because EBSD patterns fitting quality is more than enough and corresponding angle deviation in the orientation contrast is low (Fig. 3d,g,j). Therefore, local misorientation observed at the GBs is a direct consequence of the strain concentration in $BiFeO_3$ films.

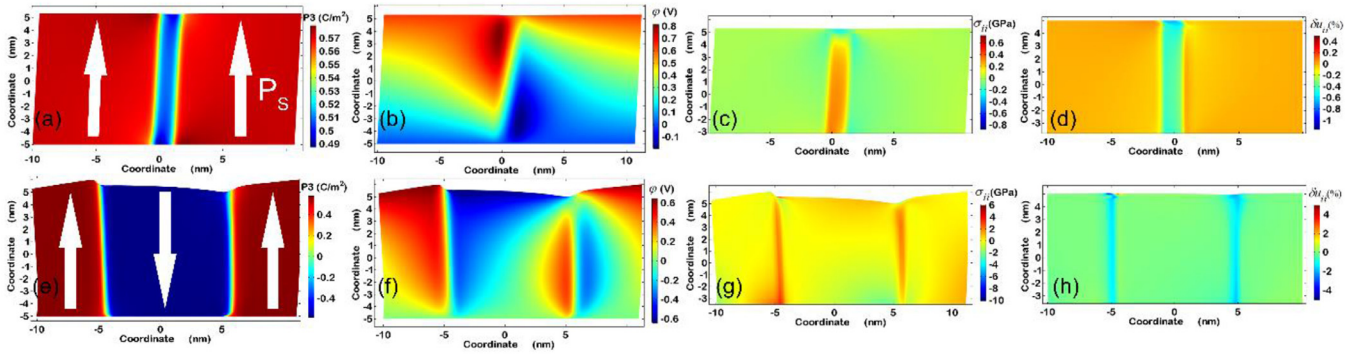

Fig. 4. Results of the FEM of the **a-d** low conductive (polarization "up-up" interface) and **e-h** highly conductive (polarization "up-down" and "down-up" interfaces) GBs in polycrystalline BFO films. **a, e** Distributions of the out-of-plane polarization component, **b, f** electrostatic potential, **c, g** hydrostatic stress near the diffuse interface, **d, h** volume expansion for the polarization "up-up" and "up-down /down-up" interfaces, respectively.

3.2. Formation mechanism of the highly conductive GBs at elevated temperature

Apparent correlation between the conductivity, polarization, and stress in thin-film BFO is not sensitive to polarization reversal at room temperature, indicating its inheritance from the earlier stage of material formation at elevated temperature. It should be mentioned that two types of GBs with different misorientation and defectiveness were observed long time ago in ferroelectric polycrystalline materials sintered in a temperature gradient [77]. In addition, temperature gradient was suggested to play a key role in the self-poling of sol-gel PZT [61] and BFO thick films [63]. The materials sintered in a temperature gradient exhibit significant difference of the dielectric permittivity, piezoelectric coefficient, and conductivity (the latter has not been shown in Ref. [77]) measured in the direction perpendicular and along the temperature gradient [77].

It is reasonable to conclude that multi-layer sol-gel BFO films around 600–700 nm thick are sublect to an unavoidable temperature gradient during cooling after synthesis. Upon cooling, domain walls in a growing polar phase take their positions tending to minimize total electrical and mechanical energy of the system [59]. Small grain size and mechanical clamping impede the formation of ferroelastic domain walls inside the grains, which should compensate the mechanical stress. As such, the films experience significant mechanical stress that can be caused not only by the thermal mismatch between the film and the substrate but also by the temperature gradient in the vertical direction. In this experimental situation, formation of the large-scale domains with aligned polarization is energetically preferable to minimize mechanical energy of the system similar to the formation of superdomains in thin films [29]. For the GBs coincident with the position of the domain walls separating the clusters, the interaction between polarization and stressed GBs via flexoelectric effect leads to a significant enhancement of the electric and elastic fields at the interface.

To evaluate the magnitude and distribution of these fields across the interfaces separating differently polarized grains, Landau-Ginsburg-Devonshire formalism was implemented and calculations were performed by the finite element modeling (FEM) simulations (Fig. 4). The details of theoretical model could be found in Supplementary Information F. Fig. 4a and 4g show the distribution of polarization variation at the interfaces between the crystallites with the different direction of spontaneous polarization. The polarization profile across the interface is inclined due to the shear strain increase near the surface, making the boundary inclined regardless the initial boundary conditions at the "nominally" plane interface. Sharp enhancement of the elastic and electric field near the interface is observed for the case of the oppositely directed polarization in the neighboring grains ("up-down" and "down-up" polarization directions) in contrast to the case of aligned polarization (Fig. 4b,f,c,g). Asymmetric elastic fields for the "up-down" and "down-up" interfaces originate from the flexoelectric effect breaking the symmetry in the direction perpendicular to the nominally uncharged interface and "charges" it [64,78,79]. It must be noted that the interfaces in real films are already slightly inclined from the substrate normal that should increase the amount of localized charge [45]. Apparent changes of the emerging electric and strain fields span at least 10 times wider (~10 nm) than the characteristic width of the interface, $L_C = 1$ nm, used in calculations, while it can be much larger in real situation. Significant stress inevitably leads to the increase of the interface width in agreement with that observed experimentally through the inspection of topography (cracks appear as a result of stress concentration) and EBSD contrasts (strain at GBs) (Fig. 3).

Accumulation of the charge at the interfaces leads to the change of the Fermi level position and, consequently, to the enhanced conductivity at that interface. Simulations predict strong enhancement by 500–2000 times of the local dc conductivity across the "up-down" and "down-up" interfaces (Supplementary Information F, Fig. F2). This is in a qualitative agreement with the obtained experimental results. However, experimentally observed current gain was much smaller: up to 30–100 times. The difference is obviously caused by the features of the C-AFM measurements, where the properties of the junction surface layer play an important role in the reduction of the captured current signal [80]. An absence of the significant current variation at "up-up" and "down-down" interfaces registered by C-AFM (Fig. 2) is also reasonably explained by the properties of the tip-sample junction..

Large electric and elastic fields localized at the GBs at elevated temperature need to be somehow screened and mobile charge defects can migrate to the area of the conductive interfaces. As the flexoeletric effect is a driving force of the conductivity at grain boundaries and it is quadratically dependent on temperature, conductive grain boundaries are likely to appear at high temperature and remain conductive upon cooling to room temperature. Therefore, polarization reversal at room temperature does not lead to the enhanced conductivity. After cooling down to room temperature, the defects conserve the conductivity along the GBs even when the domain pattern is already changed. The discovered mechanism sheds further light on the importance of the high-temperature preparation steps for the room temperature behavior of the material. Branched network of highly conductive grain boundaries should significantly impact on the electron transport in the material indirectly with Maxwell-Wagner effect [53,81] or through the enhancement of the overall leakage current [51,82,83], as well as it should influence polarization reversal [23,84]. The di-

electric measurements allow to separate DC conductivity of the grain and grain boundaries using the formalism of equivalent circuits. According to that analysis the conductivity across the grains (σ_g) was found to be much larger than conductivity of the grain boundaries (σ_{gb}): $\sigma_g \sim 10^4\sigma_{gb}$. At the same time, C-AFM measurements do not show such a pronounced difference between the grain conductivity and conductivity of the resistive GBs (intracluster GBs). This may happen because the grains and conductive (inter-cluster) GBs are connected in parallel and the interfacial capacitance is negligible, while the grain capacitance is dominant. As such, significantly higher conductivity of the grains is due to the large contribution from the conductive GBs. It should be also mentioned, that DC conductivity of the BFO films reported here is almost two orders higher than that of epitaxial BFO thin films [85] produced by sol-gel technique, and this strong increase in the conductivity may be a result of the large contribution from the presented above local mechanism.

We believe that observed effect is not specific for sol-gel BFO thin films but can be universally applied to all polycrystalline ferroelectrics. Thus, it should be considered for the understanding of the electrical properties of these, which are governed by the conductive GBs appearing at the stage of materials synthesis. It becomes even more important for the system with nanosized grains attracting great interest in applications nowadays, where the effect of multiple GBs is dominant.

4. Conclusions

The observed polarization-dependent conductivity along the GBs in polycrystalline bismuth ferrite thin films presents a new class of emerging collective phenomena in nanoscale systems. The interaction between domain walls and GBs at elevated temperature demonstrates the importance of the defect mobility in the compensation of the electric and elastic fields via depolarization field screening process. We argue that the discovery of these collective states and their response to external stress and chemical stimuli will provide further insight into the physics of complex ferroelectric oxides and may strongly affect practical applications of bismuth ferrite thin films as a material for actuators, sensors and modern nanoelectronic devices. Indeed, the observed two-orders of magnitude increase of the conductivity at the GBs provides a possibility to control the properties of ferroelectric perovskites via defect engineering and control of polarization during cooling from high temperature. This may have a significant impact on the resulting functional properties of polycrystalline ferroelectrics.

Credit author statement

Denis Alikin: Conceptualization, Methodology, Investigation, Writing - original draft, Writing - review and editing, **Saulo Portes Reis**: Investigation, Writing - review and editing, **Alexander Abramov**: Methodology, Investigation, **Dmitry Chezganov**: Methodology, Investigation, **Yevhen Fomichov**: Investigation, Writing - review and editing, **Vladimir Shur**: Resources, **Eugene Eliseev**: Investigations, **Sergei Kalinin**: Conceptualization, Writing-revie and editing, **Anna Morozovska**: Conceptualization, Methodology, Writing - review and editing, **Eudes B. Araujo**: Conceptualization, Writing - review and editing, **Andrei Kholkin**: Conceptualization, Methodology, Writing - review and editing, Resources.

Declaration of Competing Interests

None

Acknowledgments

Piezoresponse force microscopy and conductive atomic force microscopy investigations were made possible by the Russian Science Foundation (grant 19–72–10076). The equipment of the Ural Center for Shared Use “Modern nanotechnology” UrFU was used.

Part of this work was developed within the scope of the project CICECO-Aveiro Institute of Materials, UIDB/50011/2020 & UIDP/50011/2020, financed by national funds through the FCT/MEC and, when appropriate, cofinanced by FEDER under the PT2020 Partnership Agreement. For the financial support, we also express our gratitude to the Brazilian agencies: Fundação de Amparo à Pesquisa do Estado de São Paulo – FAPESP (Project N° 2017/13769–1) and Conselho Nacional de Desenvolvimento Científico e Tecnológico – CNPq (Research Grant 304604/2015–1 and Project N° 400677/2014–8) and Coordenação de Aperfeiçoamento de Pessoal de Nível Superior - CAPES (CAPES-PRINT Project: 88881.310513/2018–01). This project has received funding from the Marie Sklodowska-Curie Research and Innovation Staff Exchange program (grant agreement # 778070). Part of the work (SVK) was conducted at the Center for Nanophase Materials Sciences, which is a DOE Office of Science User Facility and supported by DOE BES scientific user facility division.

Supplementary materials

Supplementary material associated with this article can be found, in the online version, at doi:10.1016/j.apmt.2020.100740.

References

[1] J. Mannhart, D.G. Schlom, Science 327 (2010) 1607–1611.
[2] H.Y. Hwang, Y. Iwasa, M. Kawasaki, B. Keimer, N. Nagaosa, Y. Tokura, Nat. Mater. 11 (2012) 103–113.
[3] J. Socratous, S. Watanabe, K.K. Banger, C.N. Warwick, R. Branquinho, P. Barquinha, R. Martins, E. Fortunato, H. Sirringhaus, Phys. Rev. B 95 (2017) 045208.
[4] S. Nandy, G. Gonçalves, J.V. Pinto, T. Busani, V. Figueiredo, L. Pereira, R.F. Paiva Martins, E. Fortunato, Nanoscale 5 (2013) 11699.
[5] D. Schütz, M. Deluca, W. Krauss, A. Feteira, T. Jackson, K. Reichmann, Adv. Funct. Mater. 22 (2012) 2285–2294.
[6] T. Eshita, W. Wang, K. Nomura, K. Nakamura, H. Saito, H. Yamaguchi, S. Mihara, Y. Hikosaka, Y. Kataoka, M. Kojima, Jpn. J. Appl. Phys. 57 (2018) 11UA01.
[7] A.Q. Jiang, Y. Zhang, NPG Asia Mater. 11 (2019) 2.
[8] J. Seidel, L.W. Martin, Q. He, Q. Zhan, Y.-.H. Chu, A. Rother, M.E. Hawkridge, P. Maksymovych, P. Yu, M. Gajek, N. Balke, S.V. Kalinin, S. Gemming, F. Wang, G. Catalan, J.F. Scott, N.a Spaldin, J. Orenstein, R. Ramesh, Nat. Mater. 8 (2009) 229–234.
[9] P. Maksymovych, J. Seidel, Y.H. Chu, P. Wu, A.P. Baddorf, L.Q. Chen, S.V. Kalinin, R. Ramesh, Nano Lett. 11 (2011) 1906–1912.
[10] J. Seidel, P. Maksymovych, Y. Batra, A. Katan, S.-.Y. Yang, Q. He, A.P. Baddorf, S.V. Kalinin, C.-.H. Yang, J.-.C. Yang, Y.-.H. Chu, E.K.H. Salje, H. Wormeester, M. Salmeron, R. Ramesh, Phys. Rev. Lett. 105 (2010) 197603.
[11] C.T. Nelson, B. Winchester, Y. Zhang, S.J. Kim, A. Melville, C. Adamo, C.M. Folkman, S.H. Baek, C.B. Eom, D.G. Schlom, L.Q. Chen, X. Pan, Nano Lett. 11 (2011) 828–834.
[12] N. Balke, S. Choudhury, S. Jesse, M. Huijben, Y.H. Chu, A.P. Baddorf, L.Q. Chen, R. Ramesh, S.V. Kalinin, Nat. Nanotechnol. 4 (2009) 868–875.
[13] Y. Heo, J. Hong Lee, L. Xie, X. Pan, C.-.H. Yang, J. Seidel, NPG Asia Mater. 8 (2016) e297–e297.
[14] Y. Zhang, H. Lu, L. Xie, X. Yan, T.R. Paudel, J. Kim, X. Cheng, H. Wang, C. Heikes, L. Li, M. Xu, D.G. Schlom, L.-.Q. Chen, R. Wu, E.Y. Tsymbal, A. Gruverman, X. Pan, Nat. Nanotechnol. 13 (2018) 1132–1136.
[15] A. Ohtomo, H.Y. Hwang, Nature 427 (2004) 423–426.
[16] S. Thiel, Science (80-.) 313 (2006) 1942–1945.
[17] T. Sluka, A.K. Tagantsev, P. Bednyakov, N. Setter, Nat. Commun. 4 (2013) 1808.
[18] C.S. Werner, S.J. Herr, K. Buse, B. Sturman, E. Soergel, C. Razzaghi, I. Breunig, Sci. Rep. 7 (2017) 9862.
[19] A. Gruverman, O. Auciello, H. Tokumoto, Annu. Rev. Mater. Sci. 28 (1998) 101–123.
[20] D.M. Marincel, H.R. Zhang, J. Britson, A. Belianinov, S. Jesse, S.V. Kalinin, L.Q. Chen, W.M. Rainforth, I.M. Reaney, C.A. Randall, 134113 (2015) 1–12.
[21] D.M. Marincel, H. Zhang, A. Kumar, S. Jesse, S.V. Kalinin, W.M. Rainforth, I.M. Reaney, C.A. Randall, S. Trolier-McKinstry, Adv. Funct. Mater. 24 (2014) 1409–1417.
[22] B.J. Rodriguez, S. Choudhury, Y.H. Chu, A. Bhattacharyya, S. Jesse, K. Seal, A.P. Baddorf, R. Ramesh, L.-.Q. Chen, S.V. Kalinin, Adv. Funct. Mater. 19 (2009) 2053–2063.

[23] B.J. Rodriguez, Y.H. Chu, R. Ramesh, S.V. Kalinin, Appl. Phys. Lett. 93 (2008) 142901.
[24] D.O. Alikin, A.P. Turygin, J. Walker, A. Bencan, B. Malic, T. Rojac, V.Ya. Shur, A.L. Kholkin, Acta Mater. 125 (2017) 265–273.
[25] B.D. Huey, R. Nath Premnath, S. Lee, N.A. Polomoff, J. Am. Ceram. Soc. 95 (2012) 1147–1162.
[26] P. Bintachitt, S. Trolier-McKinstry, K. Seal, S. Jesse, S.V. Kalinin, Appl. Phys. Lett. 94 (2009) 042906.
[27] F. Griggio, S. Jesse, A. Kumar, D.M. Marincel, D.S. Tinberg, S.V. Kalinin, S. Trolier-McKinstry, Appl. Phys. Lett. 98 (2011) 212901.
[28] P. Bintachitt, S. Jesse, D. Damjanovic, Y. Han, I.M. Reaney, S. Trolier-McKinstry, S.V. Kalinin, Proc. Natl. Acad. Sci. U. S. A 107 (2010) 7219–7224.
[29] J.F. Scott, A. Hershkovitz, Y. Ivry, H. Lu, A. Gruverman, J.M. Gregg, Appl. Phys. Rev. 4 (2017) 041104.
[30] F. Griggio, S. Jesse, W. Qu, A. Kumar, O. Ovchinnikov, D.S. Tinberg, S.V. Kalinin, S. Trolier-McKinstry, J. Appl. Phys. 110 (2011) 044109.
[31] A. Kumar, O. Ovchinnikov, S. Guo, F. Griggio, S. Jesse, S. Trolier-McKinstry, S.V. Kalinin, Phys. Rev. B 84 (2011) 024203.
[32] O.S. Ovchinnikov, S. Jesse, P. Bintacchit, S. Trolier-McKinstry, S.V. Kalinin, Phys. Rev. Lett. 103 (2009) 157203.
[33] G. Arlt, N. a. Pertsev, J. Appl. Phys. 70 (1991) 2283–2289.
[34] S. Li, A.S. Bhalla, R.E. Newnham, L.E. Cross, Mater. Lett. 17 (1993) 21–26.
[35] G. Arlt, J. Mater. Sci. 25 (1990) 2655–2666.
[36] D. Damjanovic, M. Demartin, J. Phys. Condens. Matter 9 (1997) 4943–4953.
[37] A. Gruverman, Appl. Phys. Lett. 75 (1999) 1452–1454.
[38] Y. Kim, S. Hong, H. Park, S.H. Kim, D.K. Min, K. No, Integr. Ferroelectr. 78 (2006) 255–260.
[39] D.M. Marincel, H. Zhang, S. Jesse, A. Belianinov, M.B. Okatan, S.V. Kalinin, W.M. Rainforth, I.M. Reaney, C.A. Randall, S. Trolier-McKinstry, J. Am. Ceram. Soc. 98 (2015) 1848–1857.
[40] Y. Ivry, C. Durkan, D. Chu, J.F. Scott, Adv. Funct. Mater. 24 (2014) 5567–5574.
[41] E.A. Eliseev, A.N. Morozovska, G.S. Svechnikov, V. Gopalan, V.Y. Shur, Phys. Rev. B 83 (2011) 235313.
[42] A. Crassous, T. Sluka, A.K. Tagantsev, N. Setter, Nat. Nanotechnol. (2015) 1–6.
[43] J.P.V. McConville, H. Lu, B. Wang, Y. Tan, C. Cochard, M. Conroy, K. Moore, A. Harvey, U. Bangert, L.-.Q. Chen, A. Gruverman, J.M. Gregg, Advanced Functional Materials, John Wiley & Sons, Inc., Hoboken, NJ, USA, 2015.
[44] H. Lu, Y. Tan, J.P.V. McConville, Z. Ahmadi, B. Wang, M. Conroy, K. Moore, U. Bangert, J.E. Shield, L. Chen, J.M. Gregg, A. Gruverman, Adv. Mater. 31 (2019) 1902890.
[45] A.A. Esin, A.R. Akhmatkhanov, V.Ya. Shur, Appl. Phys. Lett. 114 (2019) 092901.
[46] B. Kirbus, C. Godau, L. Wehmeier, H. Beccard, E. Beyreuther, A. Haußmann, L.M. Eng, ACS Appl. Nano Mater. 2 (2019) 5787–5794.
[47] T. Rojac, A. Bencan, G. Drazic, N. Sakamoto, H. Ursic, B. Jancar, G. Tavcar, M. Makarovic, J. Walker, B. Malic, D. Damjanovic, Nat. Mater. 16 (2017) 322–327.
[48] H. Hu, S.B. Krupanidhi, J. Mater. Res. 9 (1994) 1484–1498.
[49] G. Gregori, R. Merkle, J. Maier, Prog. Mater. Sci. 89 (2017) 252–305.
[50] M. Imaeda, T. Mizoguchi, Y. Sato, H.S. Lee, S.D. Findlay, N. Shibata, T. Yamamoto, Y. Ikuhara, Phys. Rev. B - Condens. Matter Mater. Phys. 78 (2008) 1–12.
[51] Jang-Sik Lee, Seung-Ki Joo, Int. Semicond. Device Res. Symp. Symp. Proc. (Cat. No.01EX497) IEEE 2001 (2001) 165–168.
[52] Y.A. Genenko, O. Hirsch, P. Erhart, J. Appl. Phys. 115 (2014) 104102.
[53] T. Rojac, H. Ursic, A. Bencan, B. Malic, D. Damjanovic, Adv. Funct. Mater. 25 (2015) 2099–2108.
[54] J.L.M. Rupp, Solid State Ionics 207 (2012) 1–13.
[55] H. Simons, A.B. Haugen, A.C. Jakobsen, S. Schmidt, F. Stöhr, M. Majkut, C. Detlefs, J.E. Daniels, D. Damjanovic, H.F. Poulsen, Nat. Mater. 17 (2018) 814–819.
[56] N. Balke, S. Jesse, P. Yu, Ben Carmichael, S.V. Kalinin, A. Tselev, Nanotechnology 27 (2016) 425707.
[57] S. Bühlmann, E. Colla, P. Muralt, Phys. Rev. B - Condens. Matter Mater. Phys. 72 (2005) 1–7.
[58] D.O. Alikin, A.S. Abramov, M.S. Kosobokov, L.V. Gimadeeva, K.N. Romanyuk, V. Slabov, V.Ya. Shur, A.L. Kholkin, Calibration of the in-plane PFM response by the lateral force curves, Ferroelectrics (2020) In press.
[59] M.D. Glinchuk, E.A. Eliseev, A.N. Morozovska, Phys. Rev. B 78 (2008) 134107.
[60] S.V. Kalinin, B.J. Rodriguez, S. Jesse, J. Shin, A.P. Baddorf, P. Gupta, H. Jain, D.B. Williams, A. Gruverman, Microsc. Microanal. 12 (2006) 206–220.
[61] A.L. Kholkin, K.G. Brooks, D.V. Taylor, S. Hiboux, N. Setter, Integr. Ferroelectr. 22 (1998) 525–533.
[62] M.J. Burch, C.M. Fancher, S. Patala, M. De Graef, E.C. Dickey, Ultramicroscopy 173 (2017) 47–51.
[63] E. Khomyakova, M. Sadl, H. Ursic, J. Daniels, B. Malic, A. Bencan, D. Damjanovic, T. Rojac, ACS Appl. Mater. Interfaces 8 (2016) 19626–19634.
[64] A.N. Morozovska, R.K. Vasudevan, P. Maksymovych, S.V. Kalinin, E.A. Eliseev, Phys. Rev. B 86 (2012) 085315.
[65] M. Schrade, N. Masó, A. Perejón, L.A. Pérez-Maqueda, A.R. West, J. Mater. Chem. C 5 (2017) 10077–10086.
[66] S. Farokhipoor, B. Noheda, J. Appl. Phys. 112 (2012) 052003.
[67] A.R. Makhdoom, M.J. Akhtar, R.T.A. Khan, M.A. Rafiq, M.M. Hasan, F. Sher, A.N. Fitch, Mater. Chem. Phys. 143 (2013) 256–262.
[68] Q. Ke, X. Lou, Y. Wang, J. Wang, Phys. Rev. B 82 (2010) 024102.
[69] K. Jiang, J.J. Zhu, J.D. Wu, J. Sun, Z.G. Hu, J.H. Chu, ACS Appl. Mater. Interfaces 3 (2011) 4844–4852.
[70] D.K. Mishra, X. Qi, J. Alloys Compd. 504 (2010) 27–31.
[71] Y. Xiao, V.B. Shenoy, K. Bhattacharya, Phys. Rev. Lett. 95 (2005) 247603.
[72] L. Hong, A.K. Soh, Q.G. Du, J.Y. Li, Phys. Rev. B 77 (2008) 094104.
[73] I. Stolichnov, M. Iwanowska, E. Colla, B. Ziegler, I. Gaponenko, P. Paruch, M. Huijben, G. Rijnders, N. Setter, Appl. Phys. Lett. 104 (2014) 132902.
[74] S.V. Kalinin, Y. Kim, D.D. Fong, A.N. Morozovska, Reports Prog. Phys. 81 (2018) 036502.
[75] S.I. Wright, M.M. Nowell, Microsc. Microanal. 12 (2006) 72–84.
[76] M. Kamaya, A.J. Wilkinson, J.M. Titchmarsh, Nucl. Eng. Des. 235 (2005) 713–725.
[77] A.V. Belyaev, S.O. Kramarov, A.A. Grekov, Glas. Ceram. 46 (1989) 345–347.
[78] E.A. Eliseev, A.N. Morozovska, G.S. Svechnikov, P. Maksymovych, S.V. Kalinin, Phys. Rev. B 85 (2012) 045312.
[79] E.A. Eliseev, P.V. Yudin, S.V. Kalinin, N. Setter, A.K. Tagantsev, A.N. Morozovska, Phys. Rev. B - Condens. Matter Mater. Phys. 87 (2013) 1–9.
[80] K.N. Romanuk, D.O. Alikin, B.N. Slautin, A. Tselev, V.Ya. Shur, A.L. Kholkin (2020). arXiv:2005.00655.
[81] A.A. Esin, D.O. Alikin, A.P. Turygin, A.S. Abramov, J. Hreščak, J. Walker, T. Rojac, A. Bencan, B. Malic, A.L. Kholkin, V.Ya. Shur, J. Appl. Phys. 121 (2017) 074101.
[82] R. Waser, M. Klee, Integr. Ferroelectr. 2 (1992) 23–40.
[83] M.I. Morozov, D. Damjanovic, J. Appl. Phys. 107 (2010) 1–10.
[84] L.A. Delimova, E.V. Guschina, D.S. Seregin, K.A. Vorotilov, A.S. Sigov, J. Appl. Phys. (2017) 121.
[85] B. Yang, L. Jin, R. Wei, X. Tang, L. Hu, P. Tong, J. Yang, W. Song, J. Dai, X. Zhu, Y. Sun, S. Zhang, X. Wang, Z. Cheng, Small 3 (2019) 1903663.